

Functional Role of the “Aromatic Cage” in Human Monoamine Oxidase B: Structures and Catalytic Properties of Tyr435 Mutant Proteins^{†,‡}

Min Li,^{§,||} Claudia Binda,[⊥] Andrea Mattevi,[⊥] and Dale E. Edmondson^{*,§}

Departments of Biochemistry and Chemistry, Emory University, 1510 Clifton Road, Atlanta, Georgia 30322, and
Department of Genetics and Microbiology, University of Pavia, via Abbiategrasso 207, Pavia, 27100 Italy

Received September 11, 2005; Revised Manuscript Received March 1, 2006

ABSTRACT: Current structural results of several flavin-dependent amine oxidizing enzymes including human monoamine oxidases A and B (MAO A and MAO B) show aromatic amino acid residues oriented approximately perpendicular to the flavin ring, suggesting a functional role in catalysis. In the case of human MAO B, two tyrosyl residues (Y398 and Y435) are found in the substrate binding site on the *re* face of the covalent flavin ring [Binda et al. (2002) *J. Biol. Chem.* 277, 23973–23976]. To probe the functional significance of this structure, Tyr435 in MAO B was mutated with the amino acids Phe, His, Leu, or Trp, the mutant proteins expressed in *Pichia pastoris*, and purified to homogeneity. Each mutant protein contains covalent FAD and exhibits a high level of catalytic functionality. No major alterations in active site structures are detected on comparison of their respective crystal structures with that of WT enzyme. The relative k_{cat}/K_m values for each mutant enzyme show $\text{Y435} > \text{Y435F} = \text{Y435L} = \text{Y435H} > \text{Y435W}$. A similar behavior is also observed with the membrane-bound forms of MAO A and MAO B (MAO A Y444 mutant enzymes are found to be unstable on membrane extraction). *p*-Nitrobenzylamine is found to be a poor substrate while *p*-nitrophenethylamine is found to be a good substrate for all WT and mutant forms of MAO B. Analysis of these kinetic and structural data suggests the function of the “aromatic cage” in MAO to include a steric role in substrate binding and access to the flavin coenzyme and to increase the nucleophilicity of the substrate amine moiety. These results are consistent with a proposed polar nucleophilic mechanism for catalytic amine oxidation.

The recent structural elucidation of the recombinant human outer mitochondrial membrane enzyme monoamine oxidase B (MAO B)¹ (EC 1.4.3.4) demonstrates that its substrate binding site is composed of the *re* face of the isoalloxazine ring of the covalent FAD coenzyme with two tyrosyl residues (Y398 and Y435) occupying conformations approximately perpendicular to the flavin ring (1). These two phenolic rings are separated by 7.8 Å and adopt a conformation with one another and with the flavin as shown in Figure 1. Other flavin-dependent amine oxidases also contain aromatic amino acid side chains in similar conformations (2, 3). Maize

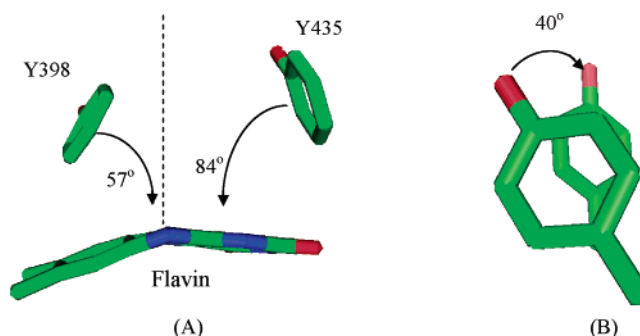


FIGURE 1: Schematic representation of the “aromatic cage” in MAO B. (A) Top view of the “aromatic cage” including the flavin ring, Y398, and Y435. The flavin ring is bent $\sim 30^\circ$ from a planar conformation. The dotted line shows the central plane of the cage. (B) Side view of the cage showing the alignment of the two tyrosyl residues. Carbon atoms are shown in green, nitrogen atoms are in blue, and oxygen atoms are in red.

[†] This work was supported by grants from the National Institute of General Medical Sciences (GM-29433) and the Ministero dell’Istruzione dell’Università e della Ricerca (FIRB, COFIN03). A.M. acknowledges support from a Pfizer Technology Development Support grant. C.B. is supported by a Young Investigator Fellowship from “Collegio Ghislieri”, Pavia.

[‡] The structures reported in this manuscript are deposited in the Protein Data Bank (<http://www.rcsb.org/pdb/>) with the codes 2c70, 2c72, 2c73, 2c75, and 2c76.

^{*} To whom correspondence should be addressed: Department of Biochemistry, Emory University, Rollins Research Bldg., 1510 Clifton Rd., Atlanta, GA 30322. E-mail: deedmon@emory.edu. Phone: 404-727-5972. Fax: 404-727-2738.

[§] Emory University.

^{||} Present address: Department of Biochemistry and Biophysics, University of California, San Francisco, 600 16th Street, San Francisco, CA 94107.

[⊥] University of Pavia.

¹ Abbreviations: MAO, monoamine oxidase; rasagiline, *N*-propargyl-1(R)aminoindan; MMTP, 1-methyl-4-(1-methyl-1*H*-pyrrol-2-yl)-1,2,3,6-tetrahydropyridine.

polyamine oxidase contains F403 and Y439 which also constitute an “aromatic cage” in front of the *re* face of the flavin ring separated by 8.2 Å (3), and bacterial trimethylamine dehydrogenase contains Y64 and W264 separated by 8.5 Å as part of an “aromatic bowl” that constitutes the substrate binding site (2). The presence of similar structures in the flavin-dependent amine oxidizing enzymes from differing sources suggests a functional role for this “aromatic cage” in the catalytic mechanism of amine oxidation by these respective enzymes.

Previous work from our laboratory (4) has shown that Phe substitutions of either of the two homologous tyrosyl residues constituting a similar aromatic cage in human MAO A (Y407 and Y444) markedly influence its catalytic properties and substrate specificities (5). A recent report shows that Y430F substitution of a component of the aromatic cage in murine polyamine oxidase results in lowered catalytic activity compared to WT enzyme (6). The structural data suggest that the role of these aromatic residues may be to orient the substrate amine moiety toward reactive sites on the flavin ring for catalysis. If this explanation were the only reason, one might expect the replacement of Tyr with Phe to have only a small effect on catalysis, which is contrary to available experimental data on two differing amine oxidases.

To date, there has been no systematic study of the structural and functional role(s) of this "aromatic cage" structure and probes of its possible role in catalysis. As an initial attempt to address this question, we have selectively mutated Y435 in MAO B with four differing amino acid side chains, expressed and purified each one to homogeneity, and examined the influence of such mutations on the catalytic properties and on the 3-dimensional structure of each mutant enzyme. The results from this study provide new insights into the role of these aromatic residues in the catalytic reductive phase of amine oxidation.

EXPERIMENTAL PROCEDURES

Construction of Y435 Mutants of MAO B and Y444 Mutants of MAO A. All site-specific mutants of MAO A were created using the Transformer site-directed mutagenesis kit (purchased from BD Bioscience Clontech, Inc.), and all mutants of MAO B were created using Quick-change site-directed mutagenesis kit (Stratagene, Inc.) based on either pUC18-HMAOA or pUC19-HMAOB. The primers for creating MAO A and MAO B mutant proteins are listed in the Supporting Information. Confirmation of the desired mutations was achieved by DNA sequence analysis by the Emory University DNA Sequencing Laboratory using an ABI Prism automated DNA sequencer.

Expression and Purification of MAO A and MAO B in *Pichia pastoris*. The *P. pastoris* (KM 71 strain) system used for the wild-type enzyme expression was also used for expression of the mutant enzymes (7, 8). All procedures used followed those described in the Invitrogen manual. MAO B Y435 mutants were purified following the same purification procedures described for wild-type protein with one modification that the polymer partition and differential centrifugation steps are replaced by a single chromatographic separation on High Q ion-exchange resin (BioRad). Of the MAO A Y444 mutants, only the Y444F mutant was sufficiently stable to solubilization and purification from the outer mitochondrial membrane fraction. Therefore, the activity studies of MAO A mutant proteins were performed using membrane particles. All expressed mutant preparations show cross reactivity to rabbit antisera raised against purified MAO A. Covalent flavin incorporation was assayed either by cross reactivity to antisera specific for covalent flavin (9) or by examining purified protein solutions after treatment with trichloroacetic acid. All purified preparations were homogeneous in SDS-PAGE and exhibit the expected masses on electrospray mass spectrometry.

Substrate Analogues. All benzylamine substrate analogues were either purchased from Sigma-Aldrich at the highest purity commercially available or synthesized as described (10). Amplex red, used to monitor H_2O_2 production in peroxidase coupled assays, was purchased from Molecular Probes, Inc. (Eugene, OR). 1-Methyl-4-(1-methyl-1*H*-pyrrol-2-yl)-1,2,3,6-tetrahydropyridine (MMTP) was used in the assay of membrane particle forms of MAO and functions with either MAO A or MAO B (11). MMTP was generously provided by Dr. Neal Castagnoli (Department of Chemistry, Virginia Polytechnic Institute and State University). The acetylenic inhibitor rasagiline was generously provided by Drs. J. Sterling and Y. Herzig (TEVA Pharm. Co., Jerusalem, Israel).

Steady-State Kinetic Experiments. All steady-state kinetic experiments were carried out at 25 °C unless stated otherwise. The reaction buffer used for assaying membrane particles contained 50 mM potassium phosphate, pH 7.5 while the buffer used for assaying solubilized enzymes was 50 mM potassium phosphate, pH 7.5, 0.5% (w/v) reduced Triton X-100. All assays were carried out in air-saturated solutions.

All spectral steady-state kinetic data were obtained using either a Lambda 2 UV-vis spectrophotometer (Perkin-Elmer Inc.) or a Cary 50 UV-vis spectrophotometer (Varian Inc.). Catalytic assays of MAO A or MAO B mutant proteins in membrane particles were performed spectrophotometrically using either MMTP (ϵ_{M} of the product is $25\,000\text{ M}^{-1}\text{ cm}^{-1}$ at 420 nm) (11) or peroxidase-coupled assays using either 4-aminoantipyrine (ϵ_{M} of the product is $4654\text{ M}^{-1}\text{ cm}^{-1}$ at 498 nm) (12) or Amplex red (ϵ_{M} of the product is $56\,000\text{ M}^{-1}\text{ cm}^{-1}$ at 560 nm) (13).

Analysis of steady-state kinetic data was performed by fitting initial velocity data to the Michaelis-Menten equation using Origin 7.0 Pro on a PC to determine turnover numbers (k_{cat}) and Michaelis constants (K_{m}). Inhibition constant values (K_{i}) were determined from the apparent K_{m} values of substrates (benzylamine for MAO B and *p*-CF₃-benzylamine for MAO A) at various inhibitor concentrations.

X-Ray Crystallography. Before crystallization experiments, the recombinant mutant proteins were incubated with 5 mM rasagiline to form their respective covalent inhibited complexes. Crystallization experiments were carried out by the sitting-drop vapor diffusion method at 4 °C (14). The protein solution contained 2 mg/mL inhibited MAO B, 8.5 mM Zwittergent 3-12, and 25 mM potassium phosphate buffer, pH 7.5. The reservoir solution consisted of 12% (w/v) PEG4000, 70 mM lithium sulfate, and 100 mM *N*-(2-acetamido)-2-iminodiacetic acid, pH 6.5.

The preparation of crystals of the *p*-nitrobenzylamine complex with MAO B followed a different protocol since this amine is a slow substrate for MAO B. Enzyme crystals were initially grown in the presence of the weak-binding reversible inhibitor *d*-amphetamine since ligand binding to the MAO B active site favors crystal formation. *p*-Nitrobenzylamine (4 mM final concentration) is then added to these crystals for ~3 min prior to transfer to a cryosolvent for freezing in liquid nitrogen. This crystal "soaking" procedure allowed the formation of the complex of *p*-nitrobenzylamine with MAO B since this analogue is bound to the enzyme with a ~10-fold higher affinity than *d*-amphetamine. Visual examination of the soaked crystals showed them to retain

Table 1: Crystallographic Data Collection and Refinement Statistics for MAO B Y435 Mutants and for the MAO B Complex with *p*-Nitrobenzylamine

	WT with <i>p</i> -nitrobenzylamine	Y435H	Y435F	Y435L	Y435W
unit cell					
<i>a</i> (Å)	130.7	130.5	140.0	131.1	131.2
<i>b</i> (Å)	222.9	222.0	222.3	222.5	223.1
<i>c</i> (Å)	86.4	85.7	86.6	86.0	86.4
resolution (Å)	15.0–2.1	15.0–2.0	15.0–2.2	15.0–1.7	15.0–1.7
$R_{\text{sym}}^{b,c}$ (%)	11.3 (30.6)	9.5 (24.0)	12.1 (52.1)	8.5 (32.6)	8.8 (39.9)
completeness ^c (%)	96.1 (91.3)	99.2 (99.9)	92.7 (93.7)	98.5 (99.4)	98.9 (99.9)
obsd refls	254 172	233 751	189 761	413 212	424 113
unique refls	74 666	83 429	62 991	134 873	136 583
multiplicity	3.4	2.8	3.0	3.1	3.1
I/σ^c	11.0 (2.7)	10.1 (3.8)	9.1 (1.1)	10.3 (2.8)	10.0 (2.4)
no. of atoms					
protein/ligand/water	8017/22/529	8013/26/354	8015/26/315	8009/26/881	8021/26//910
R_{cryst}^d (%)	18.8	20.1	23.5	18.8	19.1
R_{free}^d (%)	22.6	23.3	27.8	20.9	21.3
rmsd bond length (Å)	0.012	0.009	0.018	0.008	0.008
rmsd bond angle (deg)	1.3	1.1	1.7	1.1	1.2

^a Crystals belong to space group C222. ^b $R_{\text{sym}} = \sum |I_i - \langle I \rangle| / \sum I_i$, where I_i is the intensity of *i*th observation and $\langle I \rangle$ is the mean intensity of the reflection. ^c Values in parentheses are for reflections in the highest resolution shell. ^d $R_{\text{cryst}} = \sum |F_{\text{obs}} - F_{\text{calc}}| / \sum |F_{\text{obs}}|$ where F_{obs} and F_{calc} are the observed and calculated structure factor amplitudes, respectively. R_{cryst} and R_{free} were calculated using the working test and test set, respectively.

their yellow color, indicating that the flavin is in its oxidized form. Other experiments showed that oxidized MAO B crystals incubated with benzylamine no longer diffract. X-ray diffraction data were collected at 100 K either at the Swiss Light Source in Villigen or at the beam lines of the European Synchrotron Radiation Facility in Grenoble. For data collection, crystals were transferred into a mother liquor solution containing 18% (w/v) glycerol and flash-cooled in a stream of gaseous nitrogen at 100 K. Data processing and scaling were carried out using MOSFLM (15) and programs of the CCP4 package (16). The structure of wild-type MAO B in complex with rasagiline was used as a starting model (17) for crystallographic refinement, which was performed with the programs REFMAC5 (18) and O (19) as described (17). Refinement statistics are listed in Table 1. Cavities were identified with the program VOIDOO (20). Pictures were produced using Molscript (21) and Raster3d (22).

RESULTS

Expression of Mutant Enzymes. MAO B Y435X mutant proteins were all expressed to uniform levels in *Pichia* using protocols worked out for WT MAO B. These mutant enzymes can be solubilized from the membrane and fractionate as does WT enzyme on High Q-anion exchange columns. They exhibit slightly lower stabilities than WT enzyme although the stabilities of each of the mutant forms are sufficient to allow their purification and handling. In contrast, MAO A Y444 mutants (with the exception of the Y444F mutant) rapidly lost activity upon solubilization from the membrane, which precluded further purification and characterization. Western blot analysis of all preparations of both MAO A and MAO B mutants demonstrates that they all contain covalent flavin. Therefore the mutations at MAO B Y435 or at MAO A Y444 do not prevent the covalent incorporation of FAD.

As an example, Figure 2 shows that the absorption spectrum of MAO B Y435F is similar to that of oxidized, resting WT MAOB with an intensity corresponding to ~1 mol of FAD/60 kDa protein. The level of reduction by

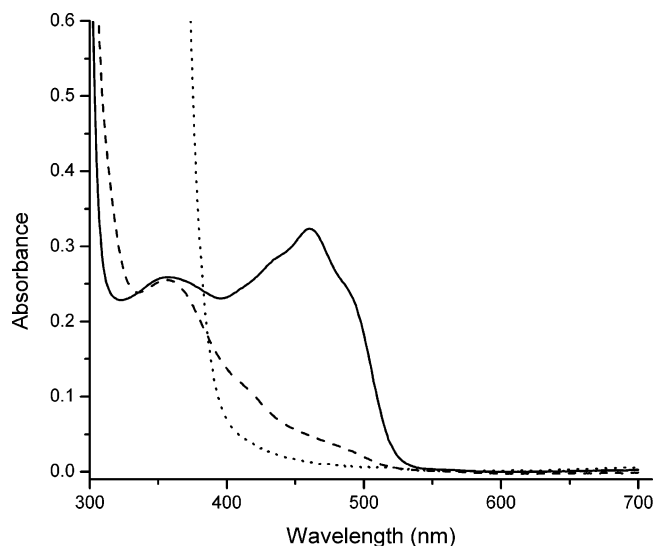


FIGURE 2: Absorption spectral properties of the bound flavin in a functionality assay of MAO BY435F mutant: (—) oxidized form; (---) after benzylamine reduction; and (···) after reduction by the addition of several crystals of sodium dithionite. All spectra were measured under an Ar atmosphere in 50 mM sodium phosphate buffer containing 0.5% (w/v) reduced Triton X-100.

substrate is extensive relative to that after chemical reduction by dithionite, which demonstrates ~80% functionality. This level or higher levels of functionality are observed for all mutant proteins. All k_{cat} values listed are based on levels of functional enzyme in each preparation. Electrospray mass spectrometry of each of the purified mutant proteins shows masses consistent with their respective mutations (data not shown). In all cases, the mutations of MAO A and of MAO B do not appear to influence their respective folding and incorporation in the outer mitochondrial membrane. The main influence of these mutations on the structural properties of MAO A is manifest in their greater labilities on solubilization from their respective membrane environments.

Catalytic Activity of MAO B Y435 Mutant Proteins. After purification, the catalytic properties of the MAO B Y435 mutant enzymes were characterized with various amine

Table 2: Steady-State Kinetic Parameters for the Oxidation of Para-Substituted Benzylamine and Phenylethylamine Analogues by Wild-Type MAO B and MAO B Y435 Mutants at 25 °C

enzyme	substrate	k_{cat} (min ⁻¹)	K_m (mM)	k_{cat}/K_m (min ⁻¹ mM ⁻¹)
WT	benzylamine	300 ± 5	0.15 ± 0.01	2000 ± 140
	<i>p</i> -CF ₃ -benzylamine	80.0 ± 0.3	0.05 ± 0.01	1600 ± 320
	<i>p</i> -NO ₂ -benzylamine	11.1 ± 0.5	0.09 ± 0.01	123 ± 15
	phenylethylamine	228.9 ± 0.9	0.016 ± 0.001	14306 ± 900
	<i>p</i> -NO ₂ -phenylethylamine	111.0 ± 2.5	0.005 ± 0.001	22200 ± 4500
Y435H	benzylamine	119.4 ± 9.9	7.2 ± 1.0	16.6 ± 2.7
	<i>p</i> -CF ₃ -benzylamine	170.8 ± 6.5	1.4 ± 0.1	122 ± 10
	<i>p</i> -NO ₂ -benzylamine	13.8 ± 0.1	0.49 ± 0.02	28.2 ± 1.2
	phenylethylamine	4.0 ± 0.1	0.29 ± 0.02	13.8 ± 1.0
	<i>p</i> -NO ₂ -phenylethylamine	108.1 ± 3.8	0.22 ± 0.02	491 ± 48
Y435F	benzylamine	108.4 ± 0.3	1.15 ± 0.16	94 ± 13
	<i>p</i> -CF ₃ -benzylamine	80.0 ± 0.2	2.0 ± 0.3	40 ± 6
	<i>p</i> -NO ₂ -benzylamine	22.8 ± 1.3	0.76 ± 0.16	30 ± 6.5
	phenylethylamine	51.9 ± 3.6	0.13 ± 0.04	399 ± 125
	<i>p</i> -NO ₂ -phenylethylamine	134 ± 3	0.05 ± 0.01	2680 ± 540
Y435L	benzylamine	38.8 ± 1.2	2.49 ± 0.18	15.6 ± 1.2
	<i>p</i> -CF ₃ -benzylamine	27.3 ± 0.9	0.99 ± 0.10	27.6 ± 2.9
	<i>p</i> -NO ₂ -benzylamine	competitive inhibitor: $K_i \sim 100 \mu\text{M}$		
	phenylethylamine	47.2 ± 2.1	0.05 ± 0.01	944 ± 193
	<i>p</i> -NO ₂ -phenylethylamine	108.7 ± 2.7	0.013 ± 0.001	8361 ± 676
Y435W	benzylamine	1.7 ± 0.6	8.8 ± 2.9	0.21 ± 0.07
	<i>p</i> -CF ₃ -benzylamine ^a	~0.23	~10	~0.023
	<i>p</i> -NO ₂ -benzylamine	activity not detectable		
	phenylethylamine	0.70 ± 0.03	0.68 ± 0.09	1.03 ± 0.14
	<i>p</i> -NO ₂ -phenylethylamine	134.6 ± 4.1	0.14 ± 0.01	961 ± 75

^a Due to the slow rate of catalysis, these kinetic constants were estimated from the concentration dependence for the rate of substrate *p*-CF₃-benzylamine reduction of the enzyme.

substrates. The data in Table 2 show the steady-state kinetic parameters of MAO B and MAO B Y435 mutants in catalyzing the oxidation of selected para-substituted benzylamine and phenylethylamine analogues. In general, the Y435 MAO B mutant proteins exhibit lower activities (either k_{cat} or k_{cat}/K_m) in comparison to the WT enzyme and the K_m values for all of the mutant enzymes are higher. Our initial analysis of these data considered whether the volume of the Y435 mutated residue might be a factor in altering the approach of the bound substrate to the active site flavin. Plots of $\ln k_{cat}/K_m$ for the various mutant enzymes versus Δvolume (the difference in volume of the phenolic ring of Tyr 435 with that of the mutant residue) exhibit a scattered relation (not shown). Therefore, within the range of residues tested, there does not appear to be a correlation of the volume of the Y435 side chain residue with catalytic activity. Further attempted correlations include the relationship of the pK_a values of para-substituted benzylamine analogues with $\ln k_{cat}/K_m$ of the WT and Y435 mutants. The results (not shown) show no correlations in activity with substrate pK_a values, which is consistent with previous data on MAO B showing that the substrate or competitive inhibitors are bound as their deprotonated forms (9). Comparisons between these MAO B mutant proteins with those of MAO A will be discussed in detail below.

Crystal Structures of MAO B Y435 Mutant Proteins. In order to interpret the observed differences among these MAO B Y435 mutant proteins in terms of catalytic efficiencies, it is important to determine whether any changes in active site structure of MAO B occurred as a result of these mutations.

Each of the mutant proteins was crystallized, and their structures were determined. Previous structural studies on wild-type MAO B show that crystals diffracting with the highest resolution were those that had been inhibited with the acetylenic inhibitor rasagiline (*N*-propargyl-1(R)-aminindan) (17). Therefore, flavin N(5) flavocyanine complexes with rasagiline were prepared with each Y435 mutant. Absorption spectral studies show that each of the mutants react with rasagiline to form the flavin N(5) flavocyanine adduct although the rates of inactivation are at least 10-fold slower than that observed with wild-type enzyme. Structural studies on these crystals show that all four Y435X mutant proteins are structurally identical with wild-type MAO B (Figure 3). The rms deviations of the C α chain conformation of each mutant from that of the wild-type MAO B–rasagiline complex are, in all cases, <0.4 Å. The structures of the active sites of these mutants are also indistinguishable with rasagiline binding in the same conformation with the only exception being the Y435H mutant where the indan ring of the bound inhibitor is slightly disordered. Aside from the amino acid substitutions, the only changes in the active site appear to be in the number and positions of those detectable water molecules.

The 2.2 Å structure of Y435F MAO B (Figure 3A) shows the Phe ring to be coplanar with the wild-type Tyr ring. The immobile bound water molecules in its active site are identical to those observed in the wild-type enzyme. A 1.7 Å resolution structure was also solved for the MAO B Y435W mutant (Figure 3D). No perturbations in the active site are found to occur with the larger indole side chain which is also coplanar with the wild-type Tyr residue. However, two of the immobile, conserved water molecules in the active site are displaced by the larger side-chain ring.

The 2.0 Å structure of MAO B Y435H (Figure 3B) shows that the conformation of the His side chain is also coplanar with the wild-type Tyr ring. Two “flipped” H435 side chain orientations differing by 180° on the χ_2 torsion angle are possible, and they are equally consistent with the electron density. In both orientations, the N ϵ 2 and N δ 1 atoms can establish H-bond interactions with surrounding water molecules. This observation indicates that the H435 side chain may adopt two alternative orientations that are likely to be equally populated. The electron density of the indan ring of the bound rasagiline is less well-defined than that found in the WT and the other mutant structures suggesting that the indan ring might not be fixed in one single conformation. Consistent with this finding is the “closed” conformation of the I199 “gate” between the entrance and substrate cavities which is in an open form in wild-type enzyme (23).

The crystal structure of the only aliphatic mutation, MAO B Y435L, was solved to a 1.7 Å resolution (Figure 3C). The Leu side chain causes little perturbation of the active site with the only difference being the branched Leu side chain displacing a water molecule from its CD1 atom. The position occupied by the Y435 hydroxyl in wild-type enzyme is now occupied by a water molecule.

Structure of the *p*-Nitrobenzylamine Complex of WT MAO B. Modeling studies suggest that the amine substrate must pass between Y398 and Y435 in MAO B to access the flavin; however, no direct evidence for this event is available. Since *p*-nitrobenzylamine is a very slow substrate for MAO B (and actually functions as a reasonable competitive inhibitor), we

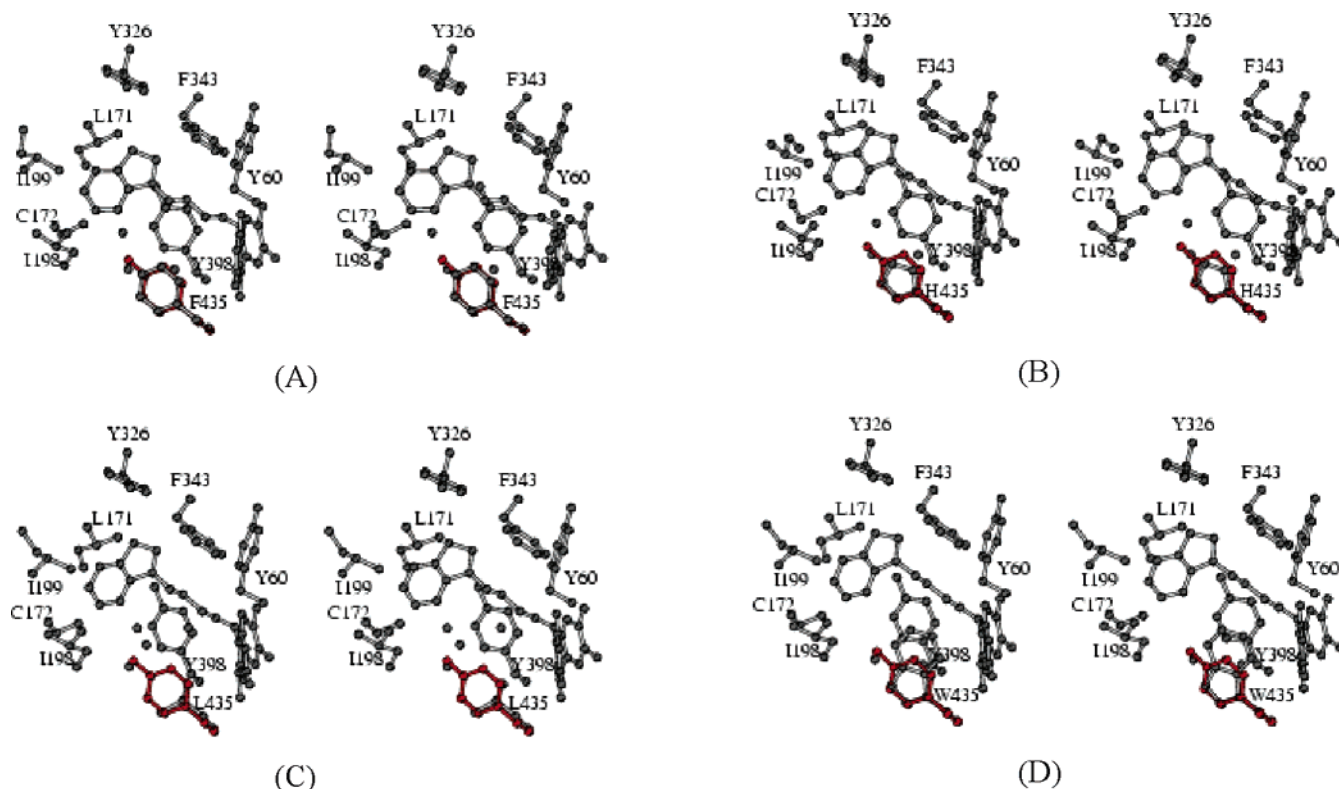


FIGURE 3: Stereoplots illustrating the structures of the rasagiline complexes of (A) Y435F, (B) Y435H, (C) Y435L, and (D) Y435W mutants of MAO B. The side chain of Tyr435 of the rasagiline complex of wild-type enzyme (red) is superimposed on the mutant structures.

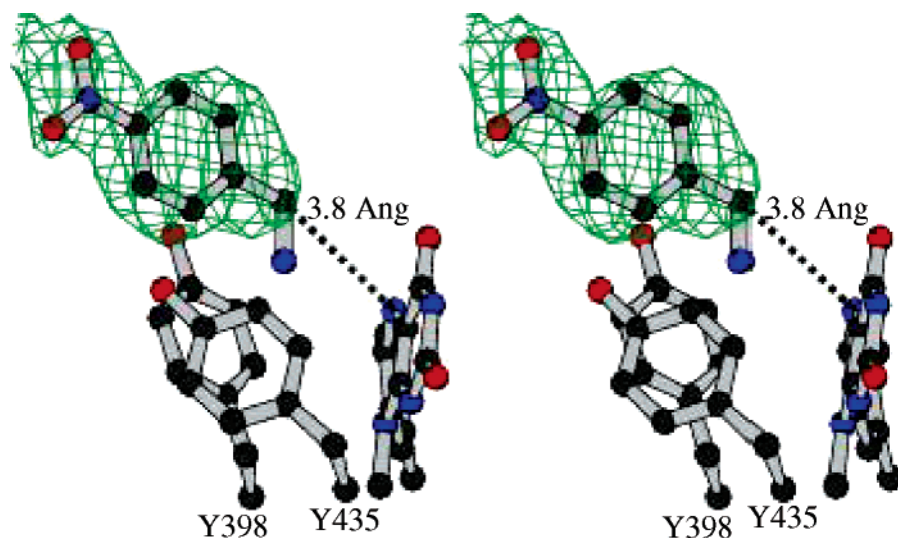


FIGURE 4: Stereoview of the position of bound *p*-nitrobenzylamine with respect to the flavin ring. The final $2F_o - F_c$ electron density map for *p*-nitrobenzylamine is shown in green (contour level 1σ).

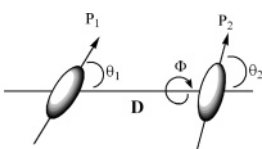
attempted to determine the structure of this substrate analogue in complex with MAO B to determine its bound orientation in the active site. Crystalline complexes of MAO B with this substrate analogue were formed as outlined in Experimental Procedures. On addition of *p*-nitrobenzylamine, the MAO B crystals exhibit no visible bleaching of their yellow color (due to flavin reduction) up to the time required (~ 3 min) to collect, mount, and freeze them for data collection. Whether turnover occurred in this experiment remains to be determined in future work using single crystal spectrophotometry. The aromatic ring, benzyl carbon side chain, and *p*-NO₂ moieties of the bound molecule could be readily

modeled in the electron density map (Figure 4) whereas the amine (or imine) N atom is not defined by the electron density. Whether this bound analogue is bound as the amine or as the imine product cannot be determined from the structural data. What can be concluded is that this nitro compound binds in the MAO B substrate binding cavity with the benzyl carbon side chain pointing toward the flavin above the space separating the phenolic rings of Y398 and Y435. The *p*-NO₂ group is coplanar with the benzene ring of the substrate. One oxygen atom of the nitro group is H-bonded to a water molecule, and the other oxygen is H-bonded to the thiol group of Cys172. The benzyl carbon is located 3.8

Å from the flavin N(5) atom. These distances compare favorably with the farnesol (a competitive inhibitor) complex with MAO B where the 1-methylene carbon is 3.4 Å from the flavin N(5) and the terminal OH group is 3.4 Å from the flavin C4a position (22).

Of interest are the differential activities exhibited by MAO B Y435 mutants with *p*-nitrobenzylamine as a substrate (Table 2). WT MAO B slowly oxidizes this substrate with a turnover number of 11 min⁻¹. *p*-Nitrobenzylamine is a competitive inhibitor for the Y435L mutant protein with weak binding ($K_i \sim 100 \mu\text{M}$) (a value 10-fold weaker than that observed for the WT enzyme). This benzylamine analogue is a substrate for the Y435H and Y435F mutants (with k_{cat}/K_m values $\sim 1/4$ that of WT enzyme). No enzymatic or inhibitory activity is detected for the Y435W mutant protein. It should be noted that *p*-nitrobenzylamine is a better substrate than benzylamine for WT human MAO A, which is proposed to be due to the electronic effects of the *p*-NO₂ substituent (10). In the case of MAO B and the Y435 mutant enzymes, the low activity observed with this substrate analogue is suggested to be due to two effects. One includes steric influences in the active site where steric and H-bonding interactions between the *p*-nitro group and the protein retard the ability of the amine moiety to form productive complexes with the covalent flavin for efficient catalysis (suggested by the structural data discussed above). The substrate binding site of MAO A differs from that of MAO B (4) and apparently allows productive complex formation without steric interference. A second effect could be due to repulsive effects of a strong dipole moment of the substrate from being placed in the same orientation as the dipoles of the two Tyr residues constituting the "aromatic cage".

Calculation of the Energy of the Dipole–Dipole Interaction between Y435 and the Substrate Amine N. Previous work from this laboratory has provided experimental support for a polar nucleophilic mechanism for MAO catalysis (10). In this mechanism, the substrate amine nitrogen is proposed to function as a nucleophile that attacks the C(4a) position of flavin cofactor as the initial step in the reductive half-reaction in MAO catalysis. It would follow that any influence that would alter the nucleophilicity of the amine N could serve to facilitate catalysis and, conversely, any effect that would decrease its nucleophilicity would result in a lowered catalytic rate. The catalytic efficiencies of the various MAO B Y435 mutant proteins are lower than that exhibited by WT enzyme (Table 2), and the structural data show no detectable conformational alterations in the active site with the various mutations. These data suggest that the environment posed by the "aromatic cage" on the substrate influences the reactivity of the amine substrate. Since the two phenolic rings of Y398 and Y435 have permanent dipole moments that are too far apart to be coupled to one another but could influence the dipole moment and/or the orientation of the bound substrate prior to reaction with the flavin, we performed simple calculations of dipole–dipole interaction energies that are expected to be altered in the Y435 mutant proteins and the amine moiety of the substrate. To simplify the calculations, these dipole moments are considered as fixed point charges and the through-space between them was approximated as a vacuum. Detailed calculations were carried out using the following equation:



$$E = - \frac{P_1 P_2 (2 \cos \theta_1 \cos \theta_2 - \sin \theta_1 \sin \theta_2 \cos \phi)}{4\pi\epsilon_0 D^3}$$

$\epsilon_0 = 8.854 \times 10^{-12}$ Faraday.meter⁻¹ (permittivity of free space)
 P = electric dipole moment (Coulomb.meter)
 D = distance between interacting atoms or molecules (meter)

To perform this calculation, coordinates from high-resolution X-ray crystal structures were used to measure the angles (θ_1 , θ_2 , and Φ) and distances (D) between the interacting moieties. Even though the "aromatic cage" includes three components (Y435, Y398, and the isoalloxazine ring of FAD), residue Y435 was considered, to a first approximation, as the only variable since the structural data show no alterations in the structures of the covalent flavin ring and the phenolic ring of Y398. Therefore, the calculation of the dipole–dipole interaction energy is based solely on the interaction between the residue 435 side chain and the substrate amino group positioned between the side chains 435 and 398. Electric dipole moment values of the amine substrates and various residue side chains were calculated using the MOPAC method in the program ChemBats3D. As shown in Figure 5, Leu and Phe side chains do not have permanent dipole moments while the side chains of Tyr, Trp, and His have permanent dipole moments with varied direction and intensity. Therefore, the interaction energies between the dipole moments of Leu and Phe side chains and that of the substrate amino group are zero while those between Tyr, Trp, and His side chains and that of the substrate amine have finite values. The dipole–dipole coupling energies for the wild type (Y435) and the four MAO B mutant enzymes (H435, W435, L435, and F435) were calculated using the above method.

The (k_{cat}/K_m) values for benzylamine oxidation by MAO B and by MAO B Y435 mutant enzymes reflect those catalytic steps up to and including the first irreversible step in catalysis. Therefore, these experimental values were correlated with the calculated interaction energies between the residue and substrate for the various mutants. Changes in (k_{cat}/K_m) values are expressed as changes in the reaction free energy ($\Delta(\Delta G^\ddagger)$) catalyzed by the MAO B Y435 mutant enzymes as compared with the wild-type MAO B. As shown in Figure 6A, a linear relationship is observed between the ratio of the catalytic rates and the calculated dipole–dipole interaction energies. Similar linear relationships are also observed using two other substrates: phenylethylamine (Figure 6A) (with a slope similar to that observed with benzylamine) and *p*-CF₃-benzylamine (Figure 6B) (with a ~ 3 -fold lower slope as compared with benzylamine). Similar analysis of *p*-nitrobenzylamine data could not be done since this compound is a substrate for some mutants and a competitive inhibitor for others (Table 2). The catalytic data for *p*-nitrophenethylamine shows a ~ 2 -fold variation of (k_{cat}/K_m) for WT MAO B and the mutants resulting in a plot as in Figure 6 with a slope of -0.3 ± 0.2 (plot not shown). The molecular basis for the observed difference in slopes will be considered in the Discussion.

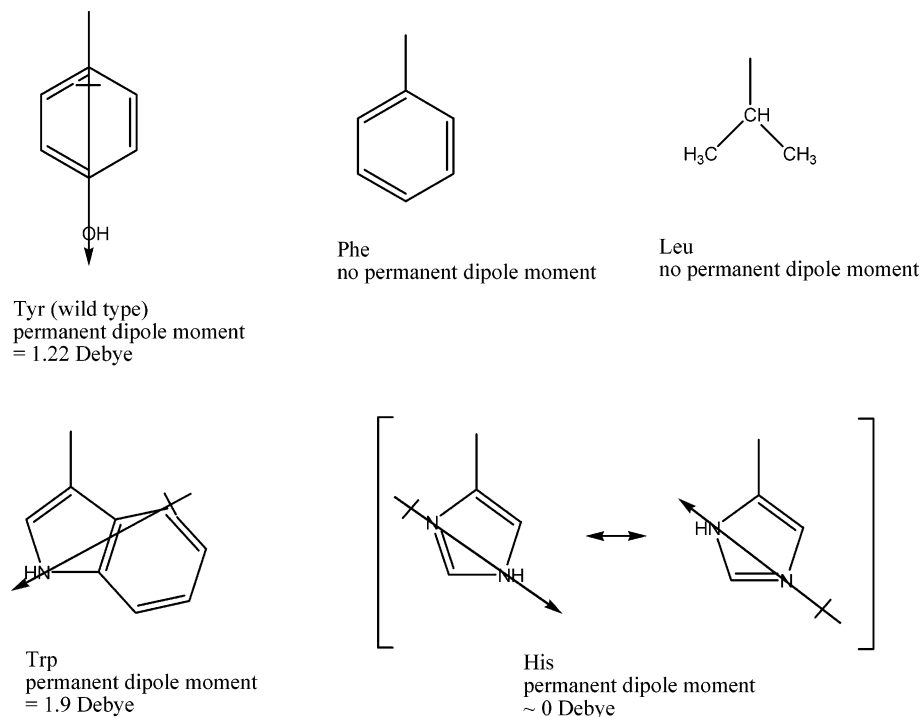


FIGURE 5: Schematic depicting the dipole moment directions for the amino acid side chains of Tyr, Trp, His, Phe, and Leu.

It should be pointed that there are two possible dipole moment directions depending on the side chain orientations of Trp and His. Based on the crystal structure, the two His side chains orientations are equally possible and each of them has two resonance structures (see Figure 5). Therefore, the net dipole moment of the imidazole side chain is approximated to be close to zero (Figure 5) with the assumption that the enzyme environment does not favor one resonance structure over the other. The orientations of the Trp indole side chain (relative to the flavin) do affect the torsion angle of the two point charges in the calculation, and therefore both dipole moment directions for the two possible orientations were used separately in initial calculations of the dipole–dipole interaction energy between this residue and the substrate amine. Only the orientation where the indole dipole moment points away from the flavin ring fits the linear plot. The X-ray crystal structure of the MAO B Y435W mutant protein shows that the indole ring orientation providing the best fit in Figure 6A,B is the one observed experimentally (Figure 3D). These combined structure and function data support the idea that the dipole–dipole interaction energy between the residue side chain at position 435 in MAO B and the substrate amino group can be correlated with the rate of enzyme catalysis.

Comparison of Catalytic Functions of MAO B Y435 and MAO A Y444 Mutant Enzymes. In order to provide some insights into whether the “aromatic cage” plays similar roles in both MAO A and MAO B, the same substrate should be utilized in order to compare the mutation effects of these two isozymes. Since the MAO A mutants could not be solubilized and purified due to their instabilities, the MMTP assay (11) was used to determine the catalytic properties of the membrane-bound forms of each of the respective mutants so that the effects of such mutations could be readily compared. This assay shows the same specificity for MAO A and MAO B, and it is readily used with membrane

preparations of these enzymes since the wavelength for observation is not readily interfered with by light scattering from the membranes (11) in spectrophotometric assays. The results of this steady-state kinetic study of all four mutants in each enzyme as well as wild-type enzymes are shown in Figure 7 as a plot of $\ln(k_{\text{cat}}/K_m)$ of MAO A Y444 and MAO B Y435 mutant proteins. If these parallel mutations of the two enzymes exhibit similar effects on catalysis, a linear correlation should be observed with a slope of 1.0. The data in Figure 7 support this expectation with a slope of 0.88 ± 0.06 ($r^2 = 0.82$) on comparison of the (k_{cat}/K_m) values of the two enzymes and their mutant forms with only the MAO A Y444H mutant enzyme exhibiting an activity departing significantly from the linear relationship. This result could be due to differences in structure of this MAO A mutant (relative to the MAO B mutant) or to differences in orientation and/or protonation of the imidazole side chain. Although the crystal structure of MAO A has recently been solved to a 3.0 Å resolution (4), further work is required to determine the structures of the mutant forms with resolutions high enough to allow the detailed calculations presented here with MAO B.

DISCUSSION

Proposed Functional Role of the Aromatic Cage in MAO Catalysis. The elucidation of the structures of several flavin-dependent amine oxidizing enzymes demonstrates the presence of aromatic residues approximately parallel to the face of the flavin where substrate binds and therefore suggests a basic functional role in flavin-dependent amine oxidation. Although this aromatic cage structure has been proposed to serve in a variety of roles such as π -cation interactions with the protonated amine substrate in trimethylamine dehydrogenase (2) or as a radical-forming intermediate in human MAO A (24), these proposed functions have not been definitively demonstrated experimentally.

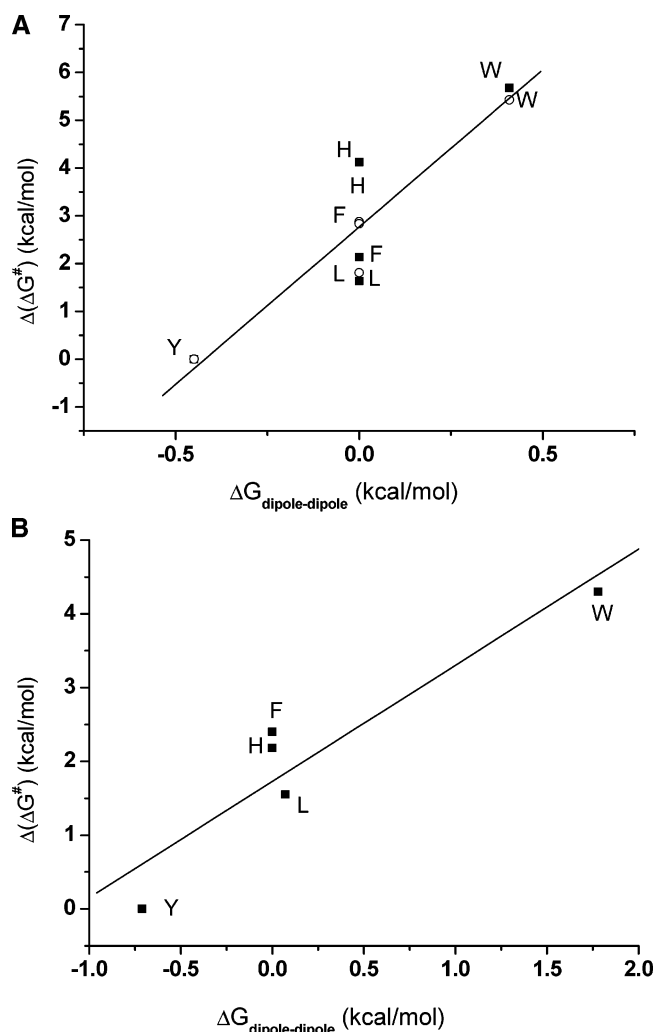


FIGURE 6: Linear relationship between the calculated interaction energy and catalytic efficiency. The abscissa ($\Delta G_{\text{dipole-dipole}}$) is the calculated dipole-dipole interaction energy between the side chain of residue 435 in various MAO B proteins and the amine moiety of the substrate. Positive and negative dipole interaction energies are the result of attraction or repulsion between two dipole moments. The ordinate ($\Delta(\Delta G^\ddagger)$) is the experimental change in reaction free energy for the four Y435 mutant enzymes compared with the wild-type MAO B. The free energy is calculated using the equation ($\Delta(\Delta G^\ddagger) = -RT \ln((V/K)^{\text{mut}}/(V/K)^{\text{wt}}$). (A) The substrates benzylamine (○) and phenylethylamine (■) fit the equation ($\Delta(\Delta G^\ddagger) = 2.7 + 6.6\Delta G_{\text{dipole-dipole}}$). (B) Substrate *p*-CF₃-benzylamine fits the equation ($\Delta(\Delta G^\ddagger) = 1.7 + 1.6\Delta G_{\text{dipole-dipole}}$).

The structural data on the MAO B Y435 mutants presented here demonstrate that alteration of this residue with either aromatic or aliphatic residues does not structurally alter the catalytic site of the enzyme. Therefore, this “aromatic cage” does not play a major structural role in maintaining the active site architecture although the mutant enzymes do exhibit lowered stabilities on solubilization from the membrane as compared to WT enzyme (a feature even more apparent with human MAO A Y444 mutant enzymes). Since the structural integrity of the active site of MAO B is not compromised by these mutations, the question now arises as to how to explain the decrease in catalytic activities of the mutant enzymes relative to that exhibited by WT enzyme.

In a previous publication (10), our laboratory has presented mechanistic evidence supporting a polar nucleophilic mechanism for MAO A catalysis as outlined in Scheme 1. The

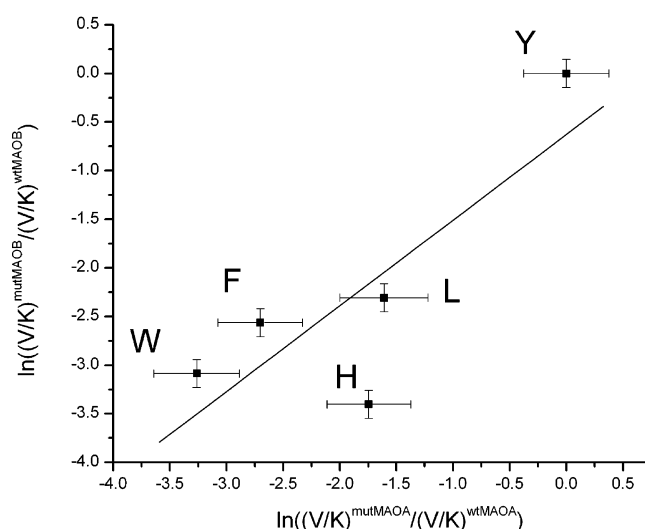
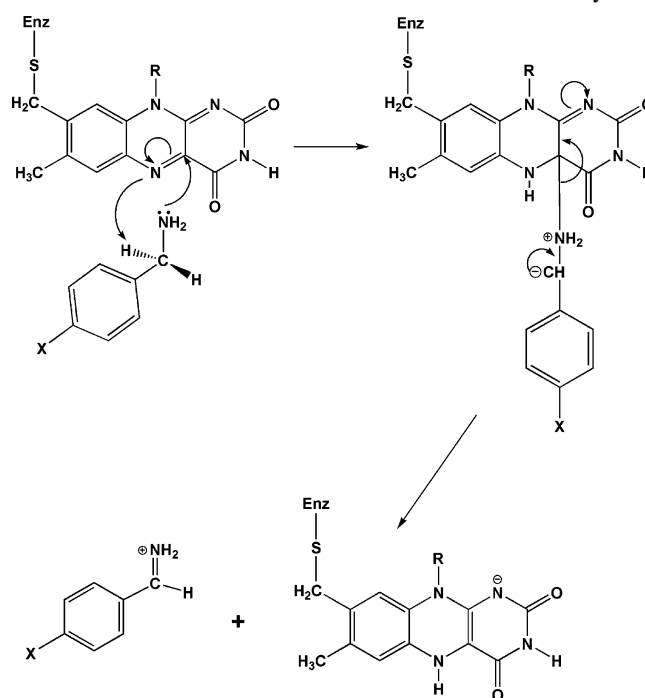


FIGURE 7: Plot of $\ln(k_{\text{cat}}/K_m)$ ratios of membrane-bound forms of Y444 MAO A mutant proteins versus $\ln(k_{\text{cat}}/K_m)$ ratios for MAO B Y435 mutant proteins. All ratios are relative to the kinetic values for the respective WT enzymes. The line represents a linear relationship between these kinetic values with a slope of 0.88 ± 0.06 . The correlation coefficient (r^2) for this plot is 0.82. If the catalytic consequences of the mutations of MAO A and MAO B were identical, a correlation with a slope of 1.0 would be observed.

Scheme 1: Proposed Polar Nucleophilic Mechanism for the Reductive Phase of Monoamine Oxidase A and B Catalysis



amine moiety of the bound substrate is in its deprotonated form and attacks the C(4a) position of the flavin to form a flavin C4a adduct. The formation of this adduct results in the generation of a basic N(5) position which subsequently abstracts the pro-*R*-H from the substrate. Recent theoretical calculations (25) support this proposed mechanism. WT MAO B does not exhibit the electronic effects on catalysis that WT MAO A does presumably due to a different conformation of the aromatic ring of the bound substrate which prevents the transmission of electronic effects from the para position to the benzyl carbon. Our hypothesis is that both enzymes follow the same mechanistic pathway. The

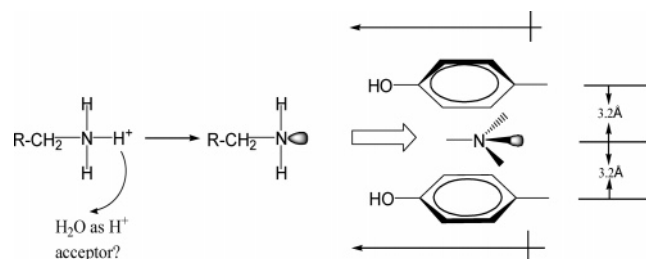


FIGURE 8: Schematic of the proposed function of the aromatic cage in amine oxidation.

structural work on MAO B and on MAO A supports this mechanistic scheme. The conformation of the flavin ring is bent rather than planar in its resting, oxidized form (26). Previous NMR studies on flavoenzymes (27) have shown that the effect of bending the flavin ring results in the N(5) exhibiting more sp^3 character (a better nucleophile) and the C(4a) position being more electrophilic (i.e. a better target for a nucleophile). In addition, recent estimates of the pK_a of the N(5) H in reduced flavin (28) (which is isoelectronic with the flavin C(4a) adduct) show it to be in the range of 24–25. Thus, the formation of the flavin C(4a) amine adduct generates a strong base at the active site for H^+ abstraction of the pro-*R* H of the substrate as suggested by a ρ value of +2 in MAO A studies (10) (no other basic residues are located in the active site that could serve as active site bases). Recent unpublished studies in this laboratory on a mutant form of MAO B also show a ρ value of +2, which supports the above suggestion that MAO A and MAO B follow similar mechanisms for amine oxidation.

Mechanistic Conclusions. From consideration of the data presented in this paper, we propose that one of the functions of the “aromatic cage” in MAO B is to provide an environment necessary to polarize the substrate amine lone pair resulting in an increase in its nucleophilicity and subsequently increasing the population of substrate molecules sufficiently activated for catalysis (Figure 8). The distance between the two phenolic rings (7.8 Å) is optimal for polarization of the amine moiety as it passes between them in the substrate binding site. Previous computational studies of the active site of MAO B by GRID analysis using $-NH_2$ as a probe (26) show the aromatic cage in front of the flavin to be energetically favorable for amine binding. Structure–activity data on amine binding to either MAO A or MAO B show the deprotonated form of the amine to be preferentially bound to the active site (9).

The data in Figure 5A show a linear relation between k_{cat}/K_m for benzylamine or phenethylamine oxidation and the calculated dipolar coupling energy between the Y435X mutation dipole and the amine dipole. A similar linear relationship (with a ~ 3 -fold lower slope than with benzylamine) is observed with *p*-CF₃-benzylamine (Figure 6B), and the slope of a similar plot for *p*-nitrophenethylamine is near zero (-0.3 ± 0.2) (plot not shown). These correlations demonstrate that a substrate with a dipole moment in the same direction as Tyr398 and Tyr435 decreases the dipolar influence of the aromatic cage. The assumption here is that other dipole–dipole effects from the other residues at the active site and the amine will remain constant. The structural data on these mutant forms of MAO B support this assumption. Thus, a reduction of dipole–dipole coupling

reduces k_{cat}/K_m for catalysis in a linear dependence. Thus, these dipolar effects of the “aromatic cage” Tyr side chains may function in a manner similar to the presence of a strong electron withdrawing group in the para position of the substrate which has been calculated (25) to decrease the amine N–flavin C(4a) distance, favoring the enhancement of charge transfer from the amine to the flavin and favoring the formation of a flavin C(4a) adduct (Scheme 1). A linear correlation is observed between the Hammett σ value for para substituents and the calculated dipole moment of the amine moiety in a series of para-substituted benzylamine analogues (see Supporting Information). Therefore, the “aromatic cage” structure apparently influences catalysis by its inductive effects on the amine nitrogen atom.

The dipole properties of Y398 and Y435 might also be expected to have a role in substrate specificity for MAO B catalysis. The data on *p*-nitro substrate analogues suggest that placing a substrate with a strong dipole moment in the same orientation as the tyrosine dipoles is akin to placing three magnets with their poles in the same direction and next to one another; resulting in repulsive interactions with substrates and therefore altering the orientation of the substrate in the active site. This repulsive effect may be one of the reasons why *p*-nitrobenzylamine is a poor substrate for MAO B although this analogue binds tightly to the active site. The kinetic data suggest that the amine moiety and the benzyl $-CH_2$ group cannot achieve a binding site structure close enough to the flavin for efficient catalysis as predicted by a polar nucleophilic mechanism. Simply increasing the length of the side chain (*p*-nitrophenylethylamine) by one methylene group now allows the direct attack on the flavin, and this substrate analogue functions well with all of the MAO B mutants. The dipole effects induced by the *p*-NO₂ substituent partially compensates for the loss of dipole coupling by the Y435 mutant forms of MAO B. A more quantitative assessment of the contributions of this aromatic cage to catalysis awaits additional experimental and computational investigations. The results presented in this paper provide, in our opinion, additional support for the proposed polar nucleophilic mechanism for MAO catalysis.

ACKNOWLEDGMENT

Dr. Neal Castagnoli (Department of Chemistry, Virginia Polytechnic Institute and State University) generously provided MMTP used in the assay, and Drs. J. Sterling and Y. Herzig at TEVA Pharm. Co. (Jerusalem, Israel) provided the acetylenic inhibitor rasagiline. We thank the Swiss Light Source in Villigen and European Synchrotron Radiation Facility beam line groups whose outstanding efforts have made these experiments possible. Ms. Milagros Aldeco provided excellent technical assistance with this project.

SUPPORTING INFORMATION AVAILABLE

Included are the list of primers used in construction of the Y444 mutants of human MAO A and characterization of mutant proteins. The characterizations include activities with different substrates, SDS PAGE Coomassie-stained gels of expressed proteins, UV/vis absorption spectra of their respective Clorgyline inhibited forms. The correlation of calculated dipole moment intensities and Hammett σ values for a series of para-substituted benzylamine analogues is also

presented. This information is available free of charge via the Internet at <http://pubs.acs.org>.

REFERENCES

1. Binda, C., Newton-Vinson, P., Hubalek, F., Edmondson, D. E., and Mattevi, A. (2002) Structure of human monoamine oxidase B, a drug target for the treatment of neurological disorders, *Nat. Struct. Biol.* 9, 22–26.
2. Trickey, P., Basran, J., Lian, L. Y., Chen, Z., Barton, J. D., Sutcliffe, M. J., Scrutton, N. S., and Mathews, F. S. (2000) Structural and biochemical characterization of recombinant wild type and a C30A mutant of trimethylamine dehydrogenase from *Methylophilus methylotrophus* (sp. W(3)A(1)), *Biochemistry* 39, 7678–7688.
3. Binda, C., Coda, A., Angelini, R., Federico, R., Ascenzi, P., and Mattevi, A. (1999) A 30-angstrom-long U-shaped catalytic tunnel in the crystal structure of polyamine oxidase, *Structure* 7, 265–276.
4. De Colibus, L., Li, M., Binda, C., Mattevi, A., and Edmondson, D. E. (2005) Three-dimensional structure of human monoamine oxidase A: Relation to the structures of rat MAO A and human MAO B, *Proc. Natl. Acad. Sci. U.S.A.* 102, 12684–12689.
5. Nandigama, R. K., Miller, J. R., and Edmondson, D. E. (2001) Loss of serotonin oxidation as a component of the altered substrate specificity in the Y444F mutant of recombinant human liver MAO A, *Biochemistry* 40, 14839–14846.
6. Royo, M., and Fitzpatrick, P. F. (2005) Mechanistic studies of mouse polyamine oxidase with N1,N12-bisethylspermine as a substrate, *Biochemistry* 44, 7079–7084.
7. Li, M., Hubalek, F., Newton-Vinson, P., and Edmondson, D. E. (2002) High-level expression of human liver monoamine oxidase A in *Pichia pastoris*: comparison with the enzyme expressed in *Saccharomyces cerevisiae*, *Protein Expression Purif.* 24, 152–62.
8. Newton-Vinson, P., Hubalek, F., and Edmondson, D. E. (2000) High-level expression of human liver monoamine oxidase B in *Pichia pastoris*, *Protein Expression Purif.* 20, 334–345.
9. Barber, M. J., Eichler, D. C., Solomonson, L. P., and Ackrell, B. A. C. (1987) Anti-flavin antibodies, *Biochem. J.* 242, 89–95.
10. Miller, J. R., and Edmondson, D. E. (1999) Structure–activity relationships in the oxidation of *para*-substituted benzylamine analogues by recombinant human liver monoamine oxidase A, *Biochemistry* 38, 13670–13683.
11. Nimkar, S. K., Mabic, S., Anderson, A. H., Palmer, S. L., Graham, T. H., de Jonge, M., Hazelwood, L., Hislop, S. J., and Castagnoli, N., Jr. (1999) Studies on the monoamine oxidase-B-catalyzed biotransformation of 4-azaaryl-1-methyl-1,2,3,6-tetrahydropyridine derivatives, *J. Med. Chem.* 42, 1828–1835.
12. Holt, A., Sharman, D. F., Baker, G. B., and Palcic, M. M. (1997) A continuous spectrophotometric assay for monoamine oxidase and related enzymes in tissue homogenates, *Anal. Biochem.* 244, 384–392.
13. Zhou, M., Diwu, Z., Panchuk-Voloshina, N., and Haugland, R. P. (1997) A stable nonfluorescent derivative of resorufin for the fluorometric determination of trace hydrogen peroxide: applications in detecting the activity of phagocyte NADPH oxidase and other oxidases, *Anal. Biochem.* 253, 162–168.
14. Binda, C., Mattevi, A., and Edmondson, D. E. (2002) Structure–function relationships in flavoenzyme-dependent amine oxidations: a comparison of polyamine oxidase and monoamine oxidase, *J. Biol. Chem.* 277, 23973–23976.
15. Leslie, A. G. (1999) Integration of macromolecular diffraction data, *Acta Crystallogr. D* 55 (Part 10), 1696–1702.
16. Collaborative Computational Project. Number 4 (1994) The CCP4 Suite: Programs for Protein Crystallography, *Acta Crystallogr. D* 50, 760–767.
17. Binda, C., Hubalek, F., Li, M., Herzig, Y., Sterling, J., Edmondson, D. E., and Mattevi, A. (2004) Crystal structures of monoamine oxidase B in complex with four inhibitors of the N-propargyl-laminoinidan class, *J. Med. Chem.* 47, 1767–1774.
18. Murshudov, G. N., Vagin, A. A., and Dodson, E. J. (1994) Refinement of macromolecular structures by the maximum-likelihood method, *Acta Crystallogr. D* 53, 240–255.
19. Jones, T. A., Zou, J. Y., Cowan, S. W., and Kjeldgaard, M. (1991) Improved methods for building protein models in electron density maps and the location of errors in these models, *Acta Crystallogr. A* 47 (Part 2), 110–119.
20. Kleywegt, G. J., and Jones, T. A. (1994) Detection, delineation, measurement, and display of cavities in macromolecular structures, *Acta Crystallogr., Sect. D: Biol. Crystallogr.* 50, 178–185.
21. Kraulis, P. J. J. (1991) MOLESCRIPT: a program to produce both detailed and schematic plots of protein structures, *J. Appl. Crystallogr.* 24, 946–950.
22. Merritt, E. A. and Bacon, D. J. (1997) Raster 3D: Photorealistic Molecular Graphics, *Methods Enzymol.* 277, 505–524.
23. Hubalek, F., Binda, C., Khalil, A., Li, M., Mattevi, A., Castagnoli, N., and Edmondson, D. E. (2005) Demonstration of isoleucine 199 as a structural determinant for the selective inhibition of human monoamine oxidase B by specific reversible inhibitors, *J. Biol. Chem.* 280, 15761–15766.
24. Rigby, S. E., Hynson, R. M., Ramsay, R. R., Munro, A. W., and Scrutton, N. S. (2005) A stable tyrosyl radical in monoamine oxidase A, *J. Biol. Chem.* 280, 4627–4631.
25. Erdem, S. S., Karahan, Ö., Yildiz, I., and Yelekçi, K. (2006) A computational study on the amine-oxidation mechanism of monoamine oxidase: Insight into the polar nucleophilic mechanism, *Org. Biomol. Chem.* 4, 646–658.
26. Binda, C., Li, M., Hubalek, F., Restelli, N., Edmondson, D. E., and Mattevi, A. (2003) Insights into the mode of inhibition of human mitochondrial monoamine oxidase B from high-resolution crystal structures, *Proc. Natl. Acad. Sci. U.S.A.* 100, 9750–9755.
27. Fleischmann, G., Lederer, F., Müller, F., Bacher, A., Ruterjans, H. (2000) Flavin-protein interactions in flavocytochrome b_2 as studied by NMR after reconstitution of the enzyme with ^{13}C - and ^{15}N -labelled flavin, *Eur. J. Biochem.* 267, 5156–5167.
28. Ghisla, S., Macheroux, P., Sanner, C., Rüterjans, H., and Müller, F. (1991) Ionisation Properties of Reduced 1,5-Dihydroflavin, Rates of N(5)-H Exchange with Solvent, in *Flavins and Flavoproteins* (Curti, B., Ronchi, S., Zanetti, G., Eds.) pp 27–32, Walter de Gruyter & Co., Berlin.

BI051847G